IOP Publishing Journal of Physics: Condensed Matter
J. Phys.: Condens. Matter **32** (2020) 195002 (6pp) https://doi.org/10.1088/1361-648X/ab6be7

A first-principles study on hydrogen distributions in the α-U/UO_2 interface

Xin-Xin Wang[1], Zi Li[1], Bingyun Ao[2], Ping Zhang[1,3], Pei Wang[1] and Yu Yang[1]

[1] LCP, Institute of Applied Physics and Computational Mathematics, Beijing 100094, People's Republic of China
[2] Science and Technology on Surface Physics and Chemistry Laboratory, Jiangyou 621908, People's Republic of China
[3] Center for Applied Physics and Technology, Peking University, Beijing 100871, People's Republic of China

E-mail: yang_yu@iapcm.ac.cn

Received 31 August 2019, revised 18 December 2019
Accepted for publication 15 January 2020
Published 13 February 2020

Abstract

We investigate the distribution preference of hydrogen in the α-U/UO_2 interface by using the DFT+U method. We find that a monolayer of hydrogen atoms firstly assembles right in the interface between α-U and UO_2. Through detailed electronic state analysis, it is revealed that the formation of U–H bonds with uranium atoms at the UO_2 side favors this hydrogen atom assembly. The newly formed U–H bonds are similar to the U–O–U superexchange interactions in UO_2. The incorporation of hydrogen in either α-U or UO_2 is much higher in energy. After formation of two hydrogen monolayers, following hydrogen atoms have no such preference in the interface area, and tend to distribute inside α-U.

Keywords: α-U/UO_2 interface, hydrogen distribution, electronic interaction, DFT+U

(Some figures may appear in colour only in the online journal)

1. Introduction

Hydrogen caused corrosion of uranium is prevalent in nuclear industry [1–8]. The hydriding reaction of uranium occurs almost spontaneously within hydrogen-sufficient environments [9, 10]. And the hydrides formed during hydrogen caused corrosion are pyrophoric and unstable, which leads to physical disintegration of uranium metals. Under the atmospheric environment of earth, uranium also has a strong affinity with oxygen or water, forming an oxide layer on top of uranium metals before hydriding occurs [11–13]. The uranium oxide layer is very dense and inert to chemical reactions with other atmospheric gases, and thus acts as a protective layer. Therefore, simulating the hydrogen caused corrosion process needs to consider a multilayer oxide/uranium system. The commonly seen stable oxide over uranium is the fluorite-like dioxide UO_2, in which uranium atoms form a face-center cubic lattice, and each oxygen atom occupies the tetrahedral center site coordinated by four uranium atoms.

Although the hydrogen corrosion of metallic uranium is closely relevant with the surface dioxide layer, the research on the interaction of hydrogen with UO_2 is still limited [14–16]. For example, it is still undetermined whether the diffusion of hydrogen is in molecular form or in atomic form. Both molecular [16] and atomic [14, 15] species have been proposed to dominate the diffusing process. Sherman and Olander believe that oxide stoichiometry and single- or poly-crystallinity notably affect the solubility of H_2 in uranium dioxide [14]. Due to the competition of impurity gases with hydrogen for sorption sites in uranium [17], the induction period of hydrides increased and the hydriding reaction rate is suppressed once the uranium exposed in H_2 with the impurity gases such as O_2, H_2O or air [18, 19]. The diffusion pathways of hydrogen are also blocked due to the gradual saturation of the oxide by the impurities [20]. Using the *ab initio* method, Flitcroft *et al* reveal that there exist stable local oxygen-rich regions that can trap and sustain high local hydrogen concentrations [21]. Harker investigates the influence of oxide thickness on

the early stages of the uranium–hydrogen reaction in experimentally, and proposes that the thinnest oxide films result in more uranium–hydrogen reaction sites and a higher mean hydrides nucleation rate. Conversely, the thickest oxide films result in fewer reaction sites and a lower mean nucleation rate [22]. Moreover, hydrogen also suppresses UO_2 corrosion in some special cases. In anoxic conditions, the combination of UO_2, synthetic groundwater, and hydrogen is able to reduce content of external oxidants entering the system and stabilize the sample surface as stoichiometric UO_2 [23].

When the dioxide (UO_2) layer forms on the metallic uranium surface, the U/UO_2 phase boundary will also have a great effect on the hydrogen caused corrosion of uranium. The study on the interaction of hydrogen with U/UO_2 phase boundary is especially deficient, which might require great attentions. Darnbrough *et al* [24] investigated the interaction between U/UO_2 bilayers and hydrogen by *in situ* x-ray diffraction. They found that small partial pressures of H_2 would cause rapid consumption of the U metal layers. Besides, the U consumption rate had a discrepancy in different orientations. According to the changes in the lattice parameters, they found that hydrogen enters both the oxide layers and metal layers, contracting the oxide and expanding the metal. They also believed that the uranium hydride layer forms on the oxide-metal interface, and the initial formation of uranium hydride lies on the defects or grain boundaries sites [24].

Despite the aforementioned experimental study on the U/UO_2 system, the theoretical investigations on the reactions of hydrogen with the U/UO_2 phase boundaries are surprisingly deficient. Here, we have constructed an α-U/UO_2 interface model and studied the distribution preference of hydrogen in the α-U/UO_2 interface using combined DFT and DFT+U methods. Our goal is to figure out the distributions of hydrogen atoms within the α-U/UO_2 phase boundary, and provide reference for future simulations on hydrogen caused corrosions of uranium.

2. Methodology

Our *ab initio* calculations are carried out by using the VASP code [25]. The electron–ion and electron–electron interactions are described by adopting the projector augmented wave method [26] and the generalized gradient approximation (GGA) with the exchange–correlation functional of Perdew–Burke–Ernzerh (PBE) [27]. The α-U/UO_2 interface is modelled by a supercell containing six atomic layers with 158 atoms (94 U atoms and 64 O atoms). The supercell size for the UO_2 side is $2*1*4$ and that for the α-U side is $2*2*4$. The collinear 1-k antiferromagnetic state is adopted for UO_2 for simplicity. The cutoff energy for the plane wave basis is set to be 400 eV. The Brillouin Zone for the interface supercell is sampled by a $3*5*1$ k-point grid using the Monkhorst–Pack method [28]. Geometry optimizations are performed until the forces on each atom are less than 0.01 eV Å^{-1}.

We treat the uranium atoms at the two sides in different ways. For α-U, since the 5f electronic states behave itinerantly after hybridizations with the 6d and 7s orbitals [29–35], we use the PBE type GGA functional to describe electronic exchange–correlation interactions. While at the UO_2 side, the 5f electrons are fully localized making UO_2 a typical Mott insulator [36–47]. We use the GGA+U method to further correct the strong electronic correlations. The quasi-annealing relaxation method [39] is adopted to avoid entering possible meta-stable states of 5f electronic configurations. We use the rotationally invariant GGA+U approach proposed by Dudarev *et al* [48–50], within which only the difference ($U_{\rm eff} = U - J$) between the on-site Coulomb parameter U and the exchange parameter J matters. In our calculations, the (U, J) values of (4.5 eV, 0.5 eV) are chosen for 5f electrons at the UO_2 side. These values have also been widely applied and proven to be reasonable for UO_2 [43–45].

The binding energy of the nth hydrogen atom in the α-U/UO_2 interface is defined as:

$$E_{\rm H}^{\rm b} = E_{\alpha\text{-}U/{\rm UO_2}+n{\rm H}} - E_{\alpha\text{-}U/{\rm UO_2}+(n-1){\rm H}} - E_{\rm H}^{\rm ref}, \qquad (1)$$

where $E_{\alpha\text{-}U/{\rm UO_2}+n{\rm H}}$ and $E_{\alpha\text{-}U/{\rm UO_2}+(n-1){\rm H}}$ are the total energies of the α-U/UO_2 interface with n and $n-1$ hydrogen atoms respectively. The reference energy $E_{\rm H}^{\rm ref}$ of hydrogen is chosen to be half the energy of a hydrogen molecule in vacuum.

3. Results and discussions

Pure uranium crystallizes into several structures, the orthorhombic α phase with four uranium atoms per unit cell at ambient conditions, followed by the body-centered tetragonal β (bct) phase at 940 K and then the body-centered cubic γ (bcc) phase at 1050 K at ambient pressure [51–53]. Here we choose the room-temperature ground-state, α-U to build the interface supercell. After full lattice relaxations, the lattice parameters of α-U and UO_2 are found to be ($a =$ 2.80 Å, $b = 5.84$ Å, $c = 4.90$ Å) and ($a = b = c = 5.53$ Å). To minimize the effects of interfacial strains coming from lattice mismatch, we build the interface along the [1 0 0] and [0 0 1] in-plane directions, for both α-U and UO_2. The in-plane size is $2*2$ for α-U, and $2*1$ for UO_2. In addition, we optimize the supercell lattice parameters fully. Along the [0 1 0] direction perpendicular to the interface, we include 4 unit cells of α-U and 4 unit cells of UO_2. After full geometry optimizations, the supercell lattice parameters become (10.48 Å, 5.58 Å, 44.71 Å). The detailed supercell geometry is shown in figure 1. As shown, we denote the four interfacial oxygen and uranium atomic layers by A, B, C, and D consequently.

Based on structure optimizations, we find that in bulk UO_2, hydrogen atom tends to occupy the octahedral center site surrounded by eight oxygen atoms, with the binding energy of 1.23 eV. Comparatively in α-U, hydrogen atom adsorbs at tetrahedral interstitial or pyramid interstitial sites. The corresponding binding energies of hydrogen are 0.30 eV and 0.33 eV. Note that we choose the reference energy for hydrogen to be half the energy of an isolated hydrogen molecule. In practical environments, the chemical potential of hydrogen is much more complicated. Therefore, the absolute

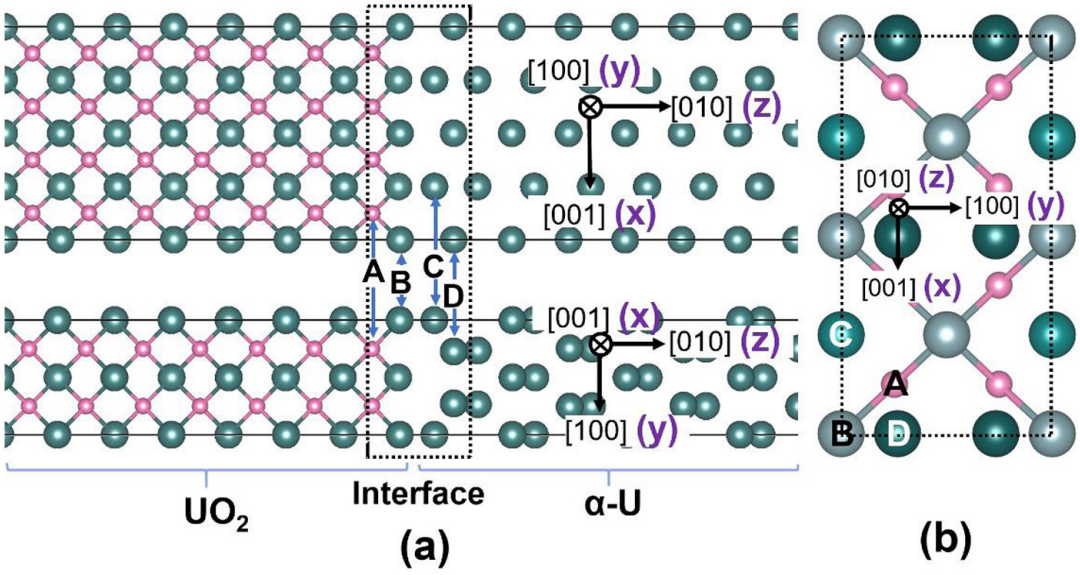

Figure 1. The configuration of the α-U/UO_2 interface from side view (a) and top view (b). The olive balls and pink balls represent for uranium and oxygen atoms respectively. In figure (b), different uranium atom layers are shown by different color depth. The interface of α-U/UO_2 phase boundary is in (1 0 1) plane for both α-U and UO_2. The different oxygen and uranium atomic layers in the boundary area are marked as A, B, C and D.

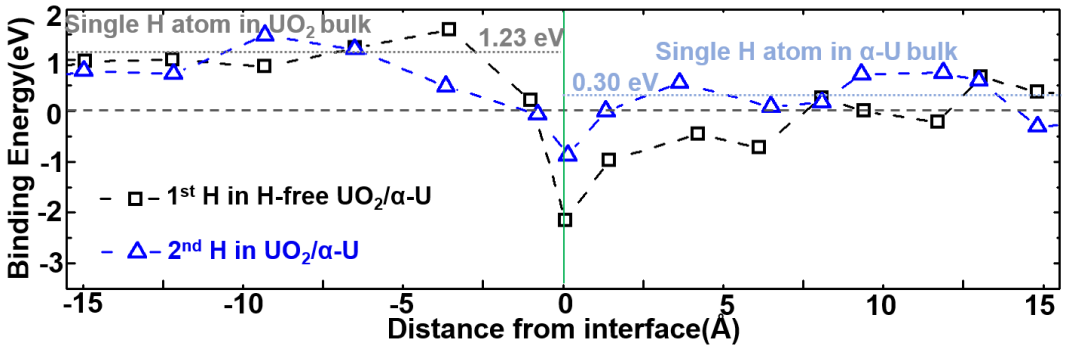

Figure 2. Binding energies of the 1st and 2nd hydrogen atom in the α-U/UO_2 interface. The left part is the UO_2 side while the right part is the α-U side. And the interface plane between α-U and UO_2 sides are depicted by the green solid line. The grey dot line is the binding energy of a single hydrogen atom in bulk UO_2 while the blue dot line is the binding energy of a single hydrogen atom in α-U.

values of the binding energies are less meaningful, and we will base our main conclusions on the relative values of the binding energies at different sites of the interface.

In the α-U/UO_2 interface, there exist adsorption sites for hydrogen between each neighboring atomic layers. To display the energetic preference of hydrogen, we calculate the binding energy of a single hydrogen atom at different sites of the interface. Figure 2 shows the obtained binding energies of the first and second hydrogen atom at different sites of the interface. For the first hydrogen atom, one can see that when it is far away from the interface plane, the binding energies are near to the values in bulk α-U and UO_2. Because there is no residual lattice strains in the ideal bulk counterparts, the small differences in the binding energies of single H between the site far away from the interface plane and that in bulk α-U or UO_2 come from the residual lattice strains at both α-U and UO_2 sides. Specifically, the stains at the α-U side are -0.06 along the [0 1 0] direction and $+0.07$ along the [0 0 1] direction respectively. And the stains at the UO_2 side are $+0.005$ along the [1 0 0] direction, $+0.01$ along the [0 1 0] direction, and -0.05 along the [0 0 1] direction. All the strains in the directions parallel to the interface are constants throughout the slabs.

Interestingly, we find that the binding energy is much lower when the first hydrogen atom stays at the interface plane, as shown in figure 2(a). It means that the first hydrogen atom is most stable when incorporated in the interface plane between the B and C atomic layers depicted in figure 1(a). Thermodynamically, the first hydrogen atom will definitely stay at the interface plane due to such a lower binding energy. Then we assume the existence of the first hydrogen atom in the interface plane, and calculate the binding energies for a second hydrogen atom. As shown in figure 2, the second hydrogen atom also has a strong tendency to stay at the interface plane as the binding energy also has a much lower value when it is incorporated in the interface plane.

By using the same method, we incorporate previous hydrogen atoms in their most stable adsorption sites, and then calculate the binding energies for the 3rd, 4th, 5th, 6th, 7th and 8th hydrogen atoms in the α-U/UO_2 interface supercell.

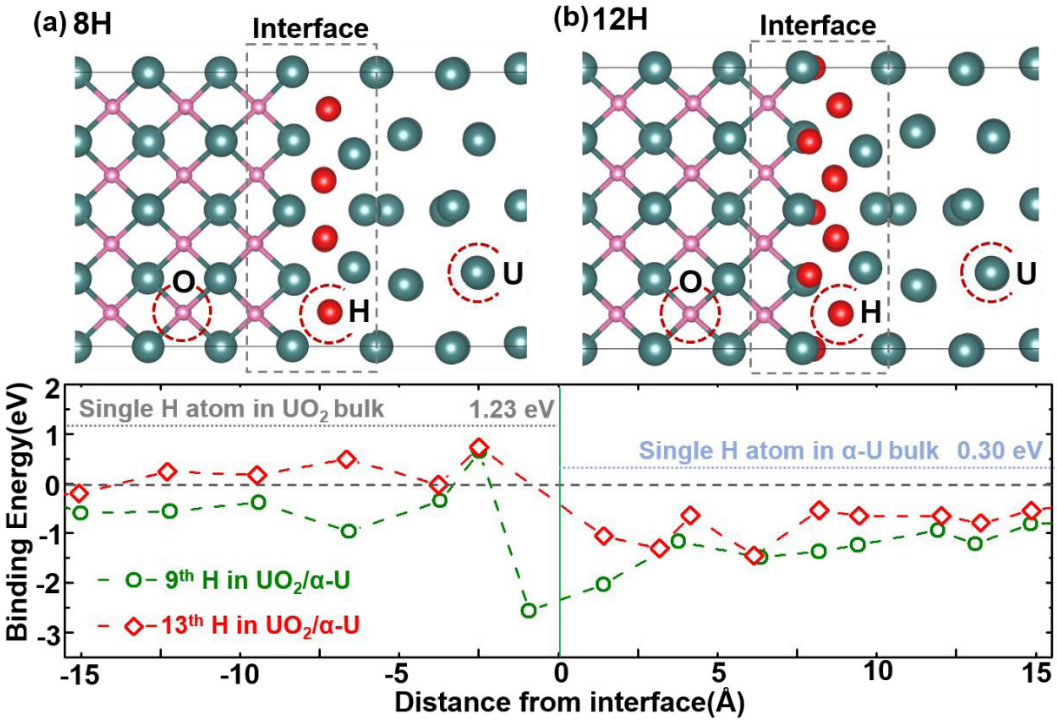

Figure 3. (a) and (b) Schematic diagrams of configuration for α-U/UO_2 interface after incorporation of eight and twelve hydrogen atoms. The olive, pink, and red balls represent uranium, oxygen, and hydrogen atoms respectively, marked by the red circles. (c) Binding energies of the 9th and 13th hydrogen atom in the α-U/UO_2 interface. The left part is the UO_2 side while the right part is the α-U side. And the interface plane between α-U and UO_2 sides are depicted by the green solid line.

We find that the binding energies for the 3rd, 4th, 5th, 6th, 7th and 8th hydrogen atom in the interface plane between layer B and layer C are always negative, and lower than that in the α-U or UO_2 area. Since there are only eight stable incorporation sites for hydrogen in the interface plane, this result means that incorporated hydrogen atoms will firstly form an atomic plane right at the boundary between α-U and UO_2. The atomic configuration of the hydrogen atomic layer between layer B and layer C is depicted in figure 3(a).

The binding energies of the 9th hydrogen atom are shown in figure 3(c). After a layer of eight hydrogen atoms forming between layer B and layer C of the α-U/UO_2 phase boundary, the binding energies of the 9th hydrogen atom is still the lowest at the interstitial site of layer B in α-U/UO_2 phase boundary. The interstitial site of layer B is closer to the UO_2 layer than the α-U layer. It indicates that the 9th hydrogen atom is the most stable at the interstitial site of layer B in α-U/UO_2 phase boundary. Besides, the binding energies of the 9th hydrogen atom in the α-U layer are all lower than that in the UO_2 layers. Note that there are only four stable incorporation sites for hydrogen in layer B. We then calculated the binding energies for the 10th, 11th, and 12th hydrogen atoms. The binding energies for the 10th, 11th, and 12th hydrogen atoms are all found to be minimum at layer B, indicating the formation of another U–H plane near the boundary plane. The configuration of this U–H plane is depicted in figure 3(b).

The red line in figure 3(c) shows the binding energies for the 13th hydrogen atom after the formation of the hydrogen and U–H planes. The result shows that there are no longer minimum values at the boundary area. And the binding energies for the 13th hydrogen atom at the α-U side are always lower than those at the UO_2 side. According to these findings, we conclude that incorporated hydrogen atoms firstly prefer to accumulate at the boundary plane, forming a hydrogen and a U–H plane, and then accumulate in the α-U region after the incorporation sites at the boundary plane are fully occupied.

To reveal underlying electronic mechanisms behind the observed hydrogen distribution rules, we then calculate and analyze the projected density of states (PDOS) for the incorporation structure of the first hydrogen atom at different sites. The PDOS distributions when the hydrogen atom is in the UO_2 and α-U regions are shown in figures 4(a) and (b) respectively, while the PDOS distributions when the hydrogen atom is in the interface plane between UO_2 and α-U are shown in figures 4(c) and (d). The U_1 and U_2 in figures 4(c) and (d) are used to denote neighboring uranium atoms at the α-U and UO_2 sides to the hydrogen atom, as shown in the insets of figure 4(d). For the incorporation in UO_2, the electronic states of hydrogen are still localized and appear to be close peaks in the PDOS distribution, as shown in figure 4(a). Similar character can also be found for hydrogen incorporated in α-U (as shown in figure 4(b)). In short words, hydrogen atoms incorporated in both α-U and UO_2 can be seen as point impurities, with very localized electronic states. While incorporated in the interface plane, a hydrogen finds a bridging site between neighboring U_1 and U_2 atoms. From the PDOS distribution shown in figures 4(c) and (d), one can see that the electronic states of H is totally broadened without any localized peaks. If we compare the electronic hybridizations between H-1s and U_2-6d/5f shown in figure 4(d), and between O-2p and U-6d/5f

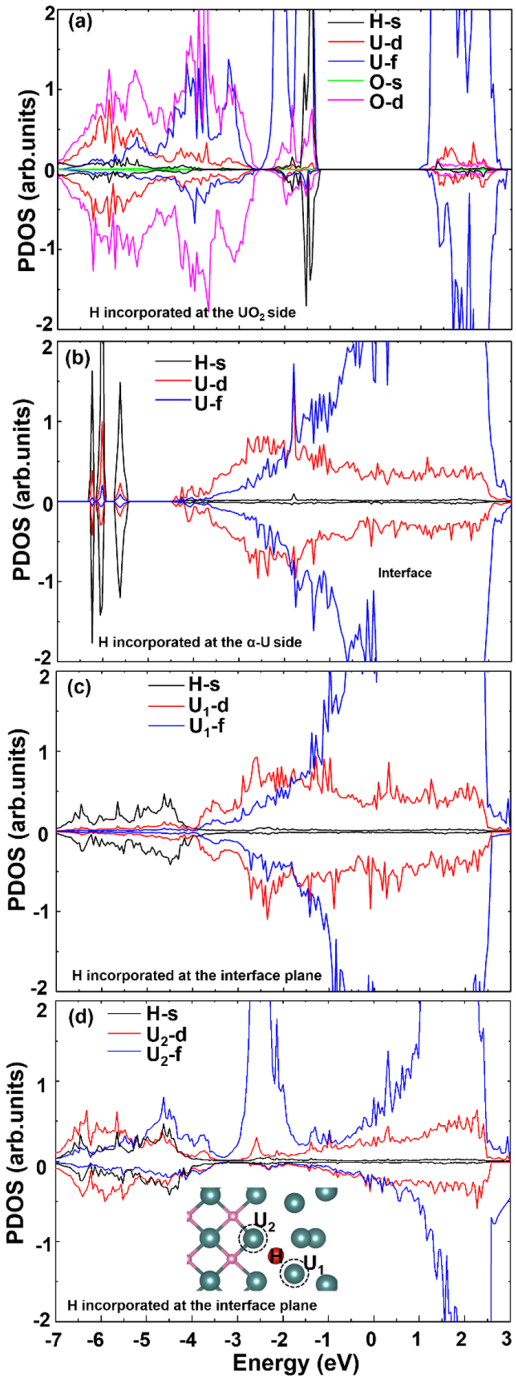

Figure 4. Projected density of states (PDOS) for the hydrogen incorporated α-U/UO_2 interface, with the hydrogen atom at the UO_2 side (a), α-U side (b), and at the interface plane (c) and (d). U_1 and U_2 denote the nearest-neighboring uranium atom to the incorporated hydrogen atom at the α-U and UO_2 sides, shown as the inset of (d). The PDOS for H-1s, O-2s, O-2p, U-5f, and U-6d states are denoted by black, green, pink, blue, and red lines. In all figures, the Fermi energy is set to be zero.

shown in figure 4(a), we can see that they are very similar. It is well known that UO_2 is an antiferromagnetic Mott insulator. There exists Ruderman–Kittel–Kasuya–Yosida type superexchange interactions between neighboring uranium atoms through bridging oxygen atoms. From the PDOS results we propose that the interfacial hydrogen atoms can act as a bridge to connect neighboring U atoms forming superexchange interaction, similar to oxygen atoms in UO_2. Somehow, from the PDOS distribution shown in figure 4(c), we see that the U_1 atom at the α-U side do not take part in the electronic hybridization with electronic states of the interfacial H atom.

4. Conclusion

In summary, by using a combined PBE and PBE + U method, and the quasi-annealing relaxation technique, we systematically investigate the hydrogen distributions in the α-U/UO_2 interface. We reveal that incorporated hydrogen atoms firstly prefer to accumulate at the interface plane region, forming two hydrogen atomic layers. After saturation, following hydrogen atoms tend to distribute at the α-U side. The binding energies of 1st–8th H atoms show that a layer of H atoms firstly forms between layer B and layer C of α-U/UO_2 phase boundary. The binding energies of 9th–12th H atoms show that once forms a layer of H atoms between layer B and layer C of the α-U/UO_2 phase boundary, they will form another layer of H atoms in the layer B of α-U/UO_2 phase boundary which is closer to the UO_2 layer. Based on electronic states analysis, we find that hydrogen atom at the interface plane can form strong U–H bonds with U atoms at the UO_2 side. The electronic states overlapping between H-1s and uranium electronic states is very similar to that between O-2p and uranium states in UO_2. Our work for the first time reveals the complicated distribution characters of hydrogen in the α-U/UO_2 interface, by predicting the formation of two hydrogen atomic layers before hydrogen accumulation inside α-U. This finding is important for further studies on hydrogen caused corrosions of uranium.

Acknowledgments

We acknowledge the computational support from the Beijing Computational Science Research Center (CSRC). This work was supported by the Science Challenge Project under Grant No. TZ2016004, the Natural Science Foundation of China under Grants No. 11974055 and No. 11847214, the Postdoctoral Science Foundation of China under Grant No. 2018M641273, the NSFC-NSAF under Grants No. U1530258 and No. U1630248.

ORCID iDs

Xin-Xin Wang https://orcid.org/0000-0001-5041-1367
Yu Yang https://orcid.org/0000-0002-1603-3603

References

[1] Condon J B and Larson E A 1973 *J. Chem. Phys.* **59** 855–65
[2] Condon J B 1975 *J. Phys. Chem.* **79** 42–8
[3] Kirkpatrlck J R 1981 *J. Phys. Chem.* **85** 3444–8
[4] Bloch J and Mintz M H 1981 *J. Less-Common Met.* **81** 301–20
[5] Mintz M H and Bloch J 1985 *Prog. Solid State Chem.* **16** 163–94
[6] Haschke J M 1998 *J. Alloys Compd.* **278** 149–60

[7] Bazley S G, Nunney T S, Mormiche C and Hayden B E 2008 *Appl. Surf. Sci.* **254** 6376–9
[8] Banos A, Harker N J and Scott T B 2018 *Corros. Sci.* **136** 129–47
[9] Arkush R, Venkert A, Aizenshtein M, Zalkind S, Moreno D, Brill M, Mintz M H and Shamir N 1996 *J. Alloys Compd.* **244** 197–205
[10] Owen L W and Scudamore R A 1996 *Corros. Sci.* **6** 461–8
[11] Allen G C and Tucker P M 1973 *J. Chem. Soc. Dalton Trans.* **5** 470–4
[12] Allen G C, Crofts J A, Curtis M T and Tucker P M 1974 *J. Chem. Soc. Dalton Trans.* **5** 1296–301
[13] Allen G C, Tucker P M and Lewis R A 1984 *J. Chem. Soc. Faraday Trans.* **80** 991–1000
[14] Sherman D F and Olander D 1989 *J. Nucl. Mater.* **166** 307–20
[15] Olander D R, Sherman D and Balooch M 1982 *J. Nucl. Mater.* **107** 31–45
[16] Wheeler V J 1971 *J. Nucl. Mater.* **40** 189–94
[17] Bloch J and Mintz M H 1997 *J. Alloys Compd.* **253–4** 529–41
[18] Alire R M, Mueller B A, Peterson C L and Mosley J R 1970 *J. Phys. Chem.* **52** 37–46
[19] Bloch J, Brami G and Kremner A 1988 *J. Alloys Compd.* **139** 371–83
[20] Teter D F, Hanrahan R J and Wetteland C J 2001 *Uranium Hydride Nucleation Kinetics: Effects of Oxide Thickness and Vacuum Outgassing* (New Mexico: Los Alamos National Laboratory)
[21] Flitcroft J M, Molinari M, Brincat N A, Williams N R, Storr M T, Allen G C and Parker S C 2018 *J. Mater. Chem.* A **6** 11362–9
[22] Harker R M 2006 *J. Alloys Compd.* **426** 106–17
[23] Carbol P, Fors P, Gouder T and Spahiu K 2009 *Geochim. Cosmochim. Acta* **73** 4366–75
[24] Darnbrough J E, Harker R M, Griffiths L, Wermeille D, Lander G H and Springell R 2018 *J. Nucl. Mater.* **502** 9–19
[25] Kresse G and Furthmüller J 1996 *Phys. Rev.* B **54** 11169–86
[26] Blöchl P E 1994 *Phys. Rev.* B **50** 17953–79
[27] Perdew J P, Burke K and Ernzerhof M 1996 *Phys. Rev. Lett.* **77** 3865–8
[28] Monkhorst H J and Pack J D 1976 *Phys. Rev.* B **13** 5188–92
[29] Gouder T 1998 *J. Alloys Compd.* **271** 841–5
[30] Huda M N and Ray A K 2005 *Int. J. Quantum Chem.* **102** 98–105
[31] Dholabhai P P and Ray A K 2007 *J. Alloys Compd.* **444–5** 356–62
[32] Yang Y, Zhang P, Shi P and Wang X L 2011 *J. Phys. Chem.* C **115** 23381–6
[33] Shi P, Yang Y, Ao B Y, Zhang P and Wang X L 2014 *J. Phys. Chem.* C **118** 26634–40
[34] Yang Y and Zhang P 2015 *J. Phys.: Condens. Matter* **27** 175005
[35] Yang Y, Liu H T and Zhang P 2016 *J. Chem. Phys.* **144** 184304
[36] Friedrich C, Schindlmayr A, Blügel S and Kotani T 2006 *Phys. Rev.* B **73** 045104
[37] Prodan I D, Scuseria G E and Martin R L 2007 *Phys. Rev.* B **76** 033101
[38] Dorado B, Amadon B, Freyss M and Bertolus M 2009 *Phys. Rev.* B **79** 235125
[39] Geng H Y, Chen Y, Kaneta Y, Kinoshita M and Wu Q 2010 *Phys. Rev.* B **82** 094106
[40] Yin Q, Kutepov A, Haule K, Kotliar G, Savrasov S Y and Pickett W E 2011 *Phys. Rev.* B **84** 195111
[41] Yu S W, Tobin J G, Crowhurst J C, Sharma S, Dewhurst J K, Olalde-Velasco P, Yang W L and Siekhaus W J 2011 *Phys. Rev.* B **83** 165102
[42] Wen X D *et al* 2012 *J. Chem. Phys.* **137** 154707
[43] Wen X D, Martin R L, Henderson T M and Scuseria G E 2013 *Chem. Rev.* **113** 1063–96
[44] Yang Y, Wang B T and Zhang P 2013 *J. Nucl. Mater.* **433** 345–50
[45] Yang Y and Zhang P 2013 *J. Appl. Phys.* **113** 013501
[46] Gilbertson S M, Durakiewicz T, Dakovski G L, Li Y W, Zhu J X, Conradson S D, Trugman S A and Rodriguez G 2014 *Phys. Rev. Lett.* **112** 087402
[47] Mo C J, Yang Y, Kang W and Zhang P 2016 *Phys. Lett.* A **380** 1481–6
[48] Dudarev S L, Manh D N and Sutton A P 1997 *Phil. Mag.* B **75** 613–28
[49] Dudarev S L, Botton G A, Savrasov S Y, Humphreys C J and Sutton A P 1998 *Phys. Rev.* B **57** 1505–9
[50] Dudarev S L, Castell M R, Botton G A, Savrasov S Y, Muggelberg C, Briggs G A D, Sutton A P and Goddard D T 2000 *Micron* **31** 363–72
[51] Koelling D D and Freeman A J 1973 *Phys. Rev.* B **7** 4454
[52] Young D A 1991 *Phase Diagrams of the Elements* (Berkeley, CA: University of California Press)
[53] Kurihara M, Hirata M, Sekine R, Onoe J and Nakamatsu H 2004 *J. Nucl. Mater.* **326** 75–9